Hindawi
Mathematical Problems in Engineering
Volume 2020, Article ID 5472502, 14 pages
https://doi.org/10.1155/2020/5472502

Research Article

Study on Vibration Characteristics of Polishing Rod for Polishing Aeroengine Blade with Abrasive Cloth Wheel

Chao Xian, Yaoyao Shi, Xiaojun Lin, and De Liu

Laboratory of Aero-engine High Performance Manufacturing, Northwestern Polytechnical University, Xi'an 710072, China

Correspondence should be addressed to Chao Xian; xianchao1994@163.com

Received 6 November 2019; Accepted 24 January 2020; Published 30 May 2020

Academic Editor: Xuping Zhang

The vibration of grinding tools is very essential to the performance of parts and the safety of machine tools. However, the vibrationis rarely studied in the process of polishing aeroengine blade with abrasive cloth wheel. Polishing force is measured by dynamometer in the process of polishing aeroengine blade with abrasive cloth wheel, and the time-domain expressions of polishing force are obtained. Time-domain and frequency-domain vibration solutions of position at which the abrasive cloth wheel is installed under the coupling of axial force and normal force are obtained by the simulation method. The results show that the total displacement is approximately equal to the displacement in the normal direction. The frequency-domain characteristics of axial force and normal force are similar. The frequency-domain characteristics of vibration in x, y, and z directions are similar. The component frequencies of polishing force are not the same as the component frequencies of rod vibration, which means the vibration is not stable. The range of spindle speed to avoid resonance in polishing process is calculated.

1. Introduction

The issue of vibration in grinding or polishing process has received considerable attentions because it plays a key role in surface quality on workpiece, processing efficiency and stability of process system However, to the author's knowledge, very few publications can be found in the literature that discuss the issue of vibration in the polishing process with an abrasive cloth wheel. This article establishes a method for analyzing the vibration characteristics of a polishing rod for polishing the aeroengine blade with an abrasive cloth wheel. In 1946, Arnold considered that the self-excited vibration caused by the decrease of the main component of cutting force relative to the cutting speed was a main reason for the chatter, and chatter is named as "friction chatter" [1]. In 1954, Inoue and Hirohito proposed that the instantaneous change of the horizontal component of cutting force lagged behind the instantaneous change of cutting thickness, which is also a reason for the self-excited vibration of cutting [2]. The self-excited vibration caused by the above lagging effect is referred to as "hysteresis chatter." Mode-coupled chatter is a kind of chatter caused by the coupling of two natural modes when the stiffness of the vibration system is similar in two directions, which was proposed by Tlusty and Ismail [3]. In the mid-1950s, Hahn published his paper "Regenerative Chatter Theory of Precision Grinding." He established the concept of regenerative chatter. He believed that the generation of grinding vibration was caused by regeneration of the ripple surface after grinding. He named it "regenerative chatter," which was the main reason of chatter [4]. Although the deep mechanism and exact theoretical model of chatter need to be further studied and discussed, the theoretical system of chatter analysis based on the above four mechanisms has been established. According to these theories, various chatter phenomenon in actual processing can be understood and explained, and it lays a theoretical foundation for suppressing chatter in production practice.

In 1984, Hashimoto et al. proposed a dynamic modeling method for cylindrical grinding based on the principle of regenerative chatter. In the stability analysis of cylindrical grinding, the effects of regenerative chatter of the workpiece and the grinding wheel on the stability of cylindrical grinding were considered, respectively [5].

From 1971 to 1985, Thompson proposed to analyze grinding stability based on the vibration equation and introduced the double regeneration effect theory [6, 7], which takes into account both the regeneration chatter of the workpiece and the grinding wheel.

In 1977, Inasaki et al. [8] studied the influence of regenerative chatter on the stability of the grinding system by establishing a mechanical model of regenerative chatter in cut-in grinding, regarding the growth rate of the surface ripple as a stability criterion. In 1987, Wardani et al. established a model describing regenerative chatter of grinding and quantitatively described the influence of grinding wheel stiffness and grinding force on grinding stability [9]. In 1997, Biera et al. established a nonlinear model in the time domain to analyze the stability of grinding process [10].

In 2001, Weck et al. modeled regenerative chatter of longitudinal grinding on the basis of the study of cut-in grinding [11]. In the same year, Inasaki et al. studied the causes of grinding chatter and the dynamics of restraining and regenerating chatter in the grinding system [12].

In 2004, Altintas et al. and Weng et al. studied the mechanics model of regenerative chatter in longitudinal grinding and surface waviness [13, 14]. In 2005, Zhang et al. established a dynamic grinding force model to analyze the relationship between grinding force and stability by resecting the geometric characteristics of the material [15]. In 2006, Li and Shin described the effect of regenerative chatter on the surface quality of the grinding wheel based on grinding stability analysis theory [16].

Li and Shin [17, 18] established several dynamic models for cylindrical grinding and then analyzed the chatter characteristics of grinding process. Yan et al. [19–25] established corresponding dynamic models for various grinding processes and analyzed grinding stability and chatter characteristics.

Li et al. [26] presented a chatter model for contour grinding. The factors affecting contour grinding, including workpiece material, Preston coefficient, and change of cutting depth during multipass grinding, were studied. Frequency response function of the machine tool structure was obtained by experiment. Then, the modal analysis was applied to the frequency response function to obtain the modal parameters which represent the mechanical structure in the chatter model.

Kabini et al. [27] established a theoretical model for predicting chatter in cylindrical grinding. The model is based on the geometric and dynamic interaction between the workpiece and the grinding wheel. The correctness of the model was verified by a series of experiments.

Entwistle and Stone [28] considered that the modeling of grinding chatter was more complex than metal cutting. This is because the number of parameters affecting the occurrence of grinding chatter is very large. In addition, unlike metal cutting, the growth of chatter in grinding may take a long time, so the growth rate is also crucial.

Hesterman and Stone [29] considered that the effect of torsional vibration on grinding chatter has been largely neglected so far. However, recent studies on cylindrical cut-in grinding show that the torsional characteristics can significantly change the system behavior and can prevent the occurrence of chatter in some cases. In order to study this problem in more detail, the frequency-domain and time-domain solutions of the cylindrical grinding model were established and these methods are described and their results are compared.

Yu et al. [30] analyzed and studied the nonlinear chatter in the grinding machine system. They regarded the grinding machine as a nonlinear multidegree-of-freedom system, and a low-dimensional system and the corresponding average equation were obtained. On the basis of deriving the average equation, the stability and bifurcation of the chatter system were discussed. It was proved that the chatter occurs in the form of Hopf bifurcation produced by the steady state of the system origin.

Cong et al. [31] studied the relationship between the dynamic characteristics of the system and the surface topography of the workpiece and established a two-degree-of-freedom (DOF) dynamic model with time-delay characteristics. Then, the Monte Carlo method and the first-order second moment method were used to analyze the fluctuation of dynamic parameters, and the reliability analysis was introduced into the flutter analysis.

Drew et al. [32] did the experiment of force change caused by the velocity oscillation of the workpiece. The results of the experiment show that the torsional vibration of the workpiece has a great influence on grinding chatter. According to the change of grinding force with workpiece speed, the change of workpiece high-frequency speed can be used to reduce chatter. Aiming at the rub-impact phenomenon of main components in the normal operation of an aeroengine, Wang et al. [33–36] studied the dynamic response of the main components in the time and frequency domains by theoretical analysis, simulation, and experimental methods.

References [37–39] gave a method to detect grinding chatter by using entropy technology.

Considering that abrasive cloth wheels have certain flexibility and can avoid underpolishing or overpolishing, Zhao et al. [40], Huai et al. [41, 42], and Xian et al. [43, 44] have proposed a method of polishing the aeroengine blade by using abrasive cloth wheels. Xiao et al. [45] presented that abrasive belt polishing was a flexible approach to polish the workpiece. However, the equipment of abrasive belt polishing is complex in mechanical structure and control.

On the one hand, because the abrasive cloth wheel is at a rotating state in polishing process, it is impossible to directly measure the vibration in all directions by using the sensor. On the other hand, it is very complicated to solve the vibration differential equation. In this paper, the polishing force for polishing aeroengine blades with abrasive cloth wheel is measured by dynamometer, and the time domain expression of polishing force is obtained by fitting. Then, the vibration solution can be obtained by simulation.

2. Experiment Device and Scheme

2.1. Experiment Equipment and Materials. In order to polish the free-form surface of the blade, the five-axis CNC

polishing machine developed by our laboratory in the experiment is designed to the five-axis linkage motion with five axes including three linear axes X, Y, and Z and two rotating axes A and C.

The channel of blisk is narrow and poor open, with mutual occlusion and wide chord curving. The tool (abrasive cloth wheel + polishing rod tool) has a good accessibility, which means the tool can process the places that other tools cannot reach. Considering that the abrasive cloth wheel can avoid underpolishing or overpolishing near the area of large curvature, the value of the wheel radius should be smaller than other occasions. So, the wheels diameter is 13.5 mm and width is 12 mm. The wheels are made of laminated adhesive resin and sand cloth whose abrasive particles are brown corundum of which the main component is alumina. The material of the polishing rod is stainless steel. The section view of the polishing rod is shown in Figure 1. The units of dimensions in the drawing are mm.

GH4169 are widely used in the aerospace industry because they have excellent comprehensive properties such as high strength, good thermal stability, strong corrosion resistance, and excellent thermal fatigue properties at high temperature, and they can work effectively for a long time at high temperature. Hence, the workpiece material of this experiment is nickel-based superalloy GH4169, and the surface of the blade was milled with a ball end milling cutter before polishing.

2.2. Experimental Principles and Procedures. Figure 2 indicates the principle of the test system. The polishing force is transmitted to the kistler 9257B-type three-direction dynamometer through the workpiece, and then the dynamometer converts the force signals into voltage signals and then inputs them into the computer through the signal amplifier and the data acquisition instrument. The dynamometer can collect the time-varying signals of force.

The rotating wheel moves transversely along a geodesic curve track of the blade surface with the workpiece fixed, which belongs to drying down polishing. Figure 3 shows the field test drawing. The dynamometer coordinate system defined with its origin located at the center of the dynamometer surface is shown in the left bottom of Figure 3. The right bottom of Figure 3 shows the polishing force signal, which is the X, Y, and Z direction polishing force signal from top to bottom on the computer screen. The acquisition frequency of the dynamometer is set to 20000 Hz.

2.3. Determination of Process Parameters. There are so many factors affecting polishing force that the effect mechanism is complicated. In this paper, the obvious effects including the spindle speed, compression depth, feed speed, and size of the abrasive cloth wheel are considered with other factors kept constant.

The maximum spindle speed of the machine tool in this experiment is 10000 r/min. For sake of the polishing efficiency and including a wide range of spindle speed, the spindle speed is selected between 4000 r/min and 8000 r/min.

Abrasive cloth wheels have certain flexibility, and the variation of the wheel radius with spindle speed is shown in Figure 4.

According to Figure 4, it can be seen that the incremental value of the wheel radius is in the range of 1 mm ~ 1.7 mm. Considering small compression depth resulting in low polishing efficiency and large compression depth making the polishing process become rigid polishing, the compression depth is selected between 0.6 mm and 1.4 mm. The feed speed is set to the range of 100 mm/min ~ 300 mm/min so that a stable polishing force signal can be acquired, and polishing effect and efficiency can be improved. The size of the abrasive cloth wheel is selected between 240# and 600# to obtain high efficiency and surface quality. The level of four factors selected in this experiment is shown in Table 1.

3. Determination of the Expression of Polishing Force

Considering the blade as the research object, F_X, F_Y, and F_Z represent the X, Y, and Z direction forces acting on the blade, respectively. The direction of F_Y is perpendicular to the paper and points to the inside of the paper.

The normal polishing force direction is the normal direction of the contact surface center in the blade surface. According to differential geometry theory, because MN is a geodesic curve, the normal line of MN coincides with the normal line of the surface. Thereby, the normal polishing force direction is the normal direction of the polishing point on MN, and the tangential polishing force direction is the tangential direction of the polishing point on MN. The normal polishing force is F_n, and the tangential polishing force is F_t as shown in Figure 5. According to the composition and decomposition of forces, normal polishing force F_n, tangential polishing force F_t, and axial force F_a can be given as

$$F_t = F_X \cos\alpha - F_Z \sin\alpha, \tag{1}$$

$$F_n = F_X \sin\alpha + F_Z \cos\alpha, \tag{2}$$

$$F_a = F_Y. \tag{3}$$

According to equations (1)–(3), time-domain signals of F_X, F_Y, and F_Z can be converted to time-domain signals of F_t, F_a, and F_n. Because F_X, F_Y, and F_Z are periodic signals, F_t, F_a, and F_n are also periodic signals. Figure 6 shows one-cycle signals of F_t, F_a, and F_n under certain process parameters.

According to the characteristics of these signals, they can be decomposed into the sum of trigonometric series signals. F_a and F_n can be expressed as

$$F_a = \sum_{i=1}^{\infty} a_i \sin\left(b_i t + c_i\right), \tag{4}$$

$$F_n = \sum_{i=1}^{\infty} \alpha_i \sin\left(\beta_i t + \gamma_i\right), \tag{5}$$

where $a_i, b_i, c_i, \alpha_i, \beta_i, \gamma_i$, $(i = 1, 2, \ldots)$ are the coefficients.

When the first eight terms of the series are taken, the fitting accuracy is relatively high. So, the first eight terms of

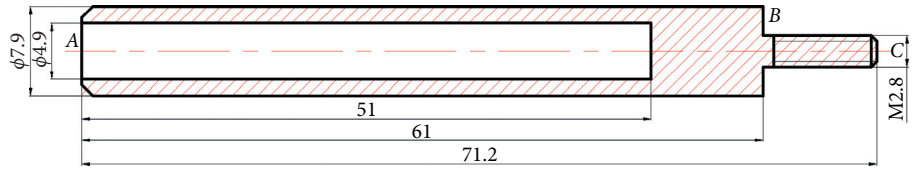

Figure 1: Section view of the part of the polishing rod hanging out.

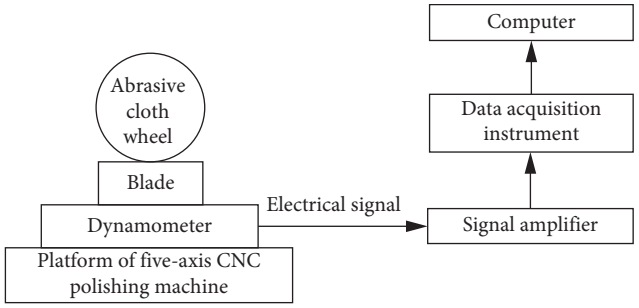

Figure 2: Schematic diagram of the test system.

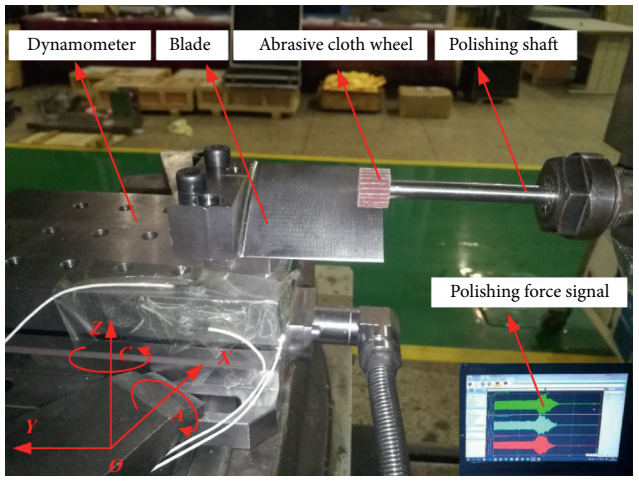

Figure 3: Test site map.

the series are taken as the expression of the force F_a and F_n. The fitting curve of F_a and F_n is shown in Figures 7 and 8.

The fitting curve equations of F_a and F_n are given as

$$\begin{aligned} F_a &= \sum_{i=1}^{8} a_i \sin(b_i t + c_i) \\ &= 14.5\sin(9492t + 1.255) + 11.78\sin(12580t + 0.0007) \\ &\quad + 15\sin(10510t + 2.635) + 7.521\sin(10120t + 1.934) \\ &\quad + 6.661\sin(8042t - 0.8875) \\ &\quad + 7.298\sin(13060t + 0.9207) \\ &\quad + 5.961\sin(12040t - 2.501) + 3.771\sin(9018t + 2.18), \end{aligned} \tag{6}$$

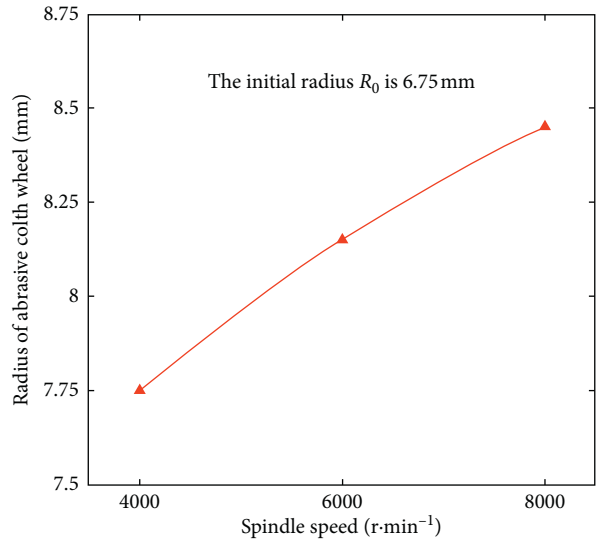

Figure 4: Variation of the radius of the abrasive cloth wheel with spindle speed.

Table 1: Test factors and horizontal distribution.

Factors		Levels		
		1	2	3
1	N	4000	6000	8000
2	a_p	0.6	1.0	1.4
3	v_w	100	200	300
4	P	240	400	600

$$\begin{aligned} F_n &= \sum_{i=1}^{8} \alpha_i \sin(\beta_i t + \gamma_i) \\ &= 9.912\sin(12480t + 1.611) + 4.97\sin(211.6t + 0.2851) \\ &\quad + 10.18\sin(10420t - 1.598) + 5.492\sin(10110t + 2.221) \\ &\quad + 9.062\sin(9461t - 2.628) + 4.463\sin(11760t - 0.1892) \\ &\quad + 3.826\sin(11100t - 0.08997) + 3.248\sin(8040t + 1.191). \end{aligned} \tag{7}$$

The right bottom of Figures 7 and 8 displays the fit goodness of F_a and F_n. The R^2 and adjusted R^2 are very close to 1, which shows that the fitting equation has a very good fitting degree and high validity.

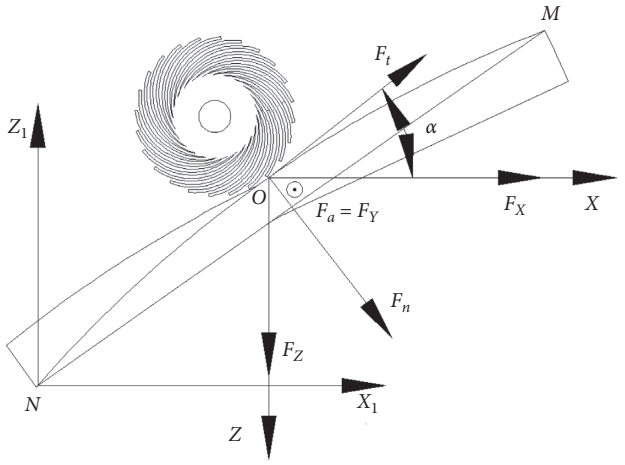

Figure 5: Schematic diagrams for calculating normal and tangential polishing forces.

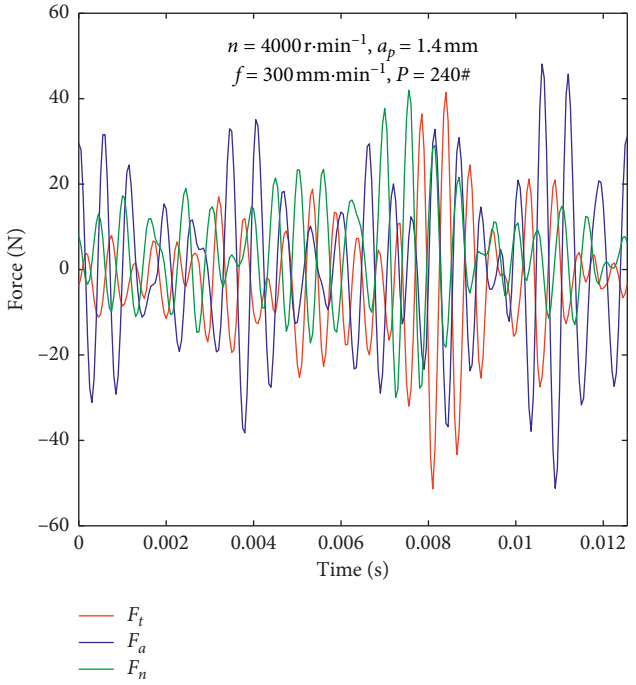

Figure 6: Time-domain signals F_t, F_a, and F_n under certain process parameters.

4. Establishment of Vibration Differential Equation

In the experiment, the vibration of the abrasive cloth wheel is considered as the vibration at the midpoint on BC as in Figure 1. The polishing rod can be regarded as a cantilever beam, and the vibration model rod and the coordinate system *o-xyz* are established, which is shown in Figure 9.

The axial forced vibration equation of the polishing rod is expressed by

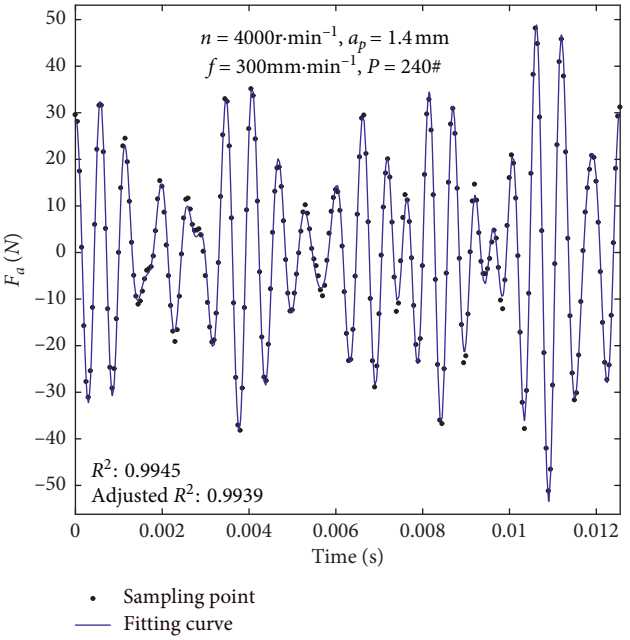

Figure 7: Fitting curve of F_a.

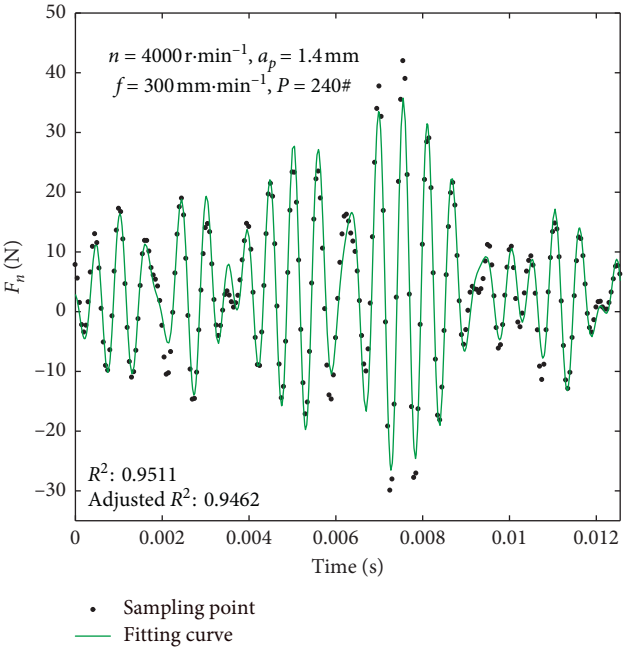

Figure 8: Fitting curve of F_n.

$$\frac{\partial}{\partial x}\left[EA(x)\frac{\partial u(x,t)}{\partial x}\right] + F_a(x,t) = \rho A(x)\frac{\partial^2 u(x,t)}{\partial t^2}. \quad (8)$$

The normal forced vibration equation of the polishing rod is

$$\frac{\partial^2}{\partial x^2}\left[EI(x)\frac{\partial^2 w(x,t)}{\partial x^2}\right] + \rho A(x)\frac{\partial^2 w(x,t)}{\partial t^2} = F_n(x,t). \quad (9)$$

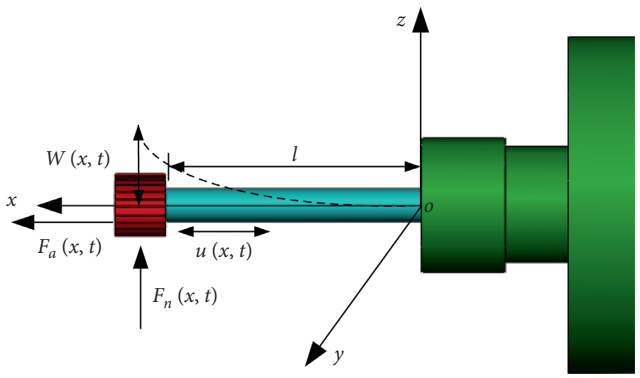

Figure 9: Vibration model.

Submitting equations (6) and (7) into equations (8) and (9), the vibration equation can be derived as

$$\frac{\partial}{\partial x}\left[EA(x)\frac{\partial u(x,t)}{\partial x}\right]+\sum_{i=1}^{\infty}a_i\sin\left(b_it+c_i\right)=\rho A(x)\frac{\partial^2 u(x,t)}{\partial t^2}, \tag{10}$$

$$\frac{\partial^2}{\partial x^2}\left[EI(x)\frac{\partial^2 w(x,t)}{\partial x^2}\right]+\rho A(x)\frac{\partial^2 w(x,t)}{\partial t^2}=\sum_{i=1}^{\infty}\alpha_i\sin\left(\beta_it+\gamma_i\right). \tag{11}$$

For one thing, the expressions of axial polishing force and normal polishing force are complex and the cross-section of the polishing rod is not equal, and solving equations (10) and (11) is very complex. For another thing, it is difficult to obtain the vibration solution under the coupling of axial force and normal force by the analytical method. So, the simulation method can be used for solving the vibration of the polishing rod.

5. Solutions of Finite Element Simulation

The simulation steps are shown in Figure 10. First, the three-dimensional model of the polishing rod is established. Second, meshing is applied and grid size is 1 mm. Third, constraint is imposed on the model, which is fixing the right end face of the polishing rod. The loads comprise of F_a and F_n, which are imposed simultaneously. Imposing axial force F_a is shown in Figure 11, and imposing normal force F_n is shown in Figure 12. Lastly, solving is proceeded. Then, the solutions can be obtained under the coupling of the two loads by simulation.

Abrasive cloth wheel is installed on the BC section as in Figure 1 by thread, and the vibration characteristics at the midpoint on BC can reflect the vibration characteristics of the abrasive cloth wheel. The solution in the x direction at the midpoint on BC is displayed in Figure 13, and solution in the z direction is displayed in Figure 14, and solution in the y direction is displayed in Figure 15. The vibration displacement curve at the midpoint on BC is shown in Figure 16.

Figure 16 shows that displacement in the normal direction (z direction) reaches 10^{-4} m, which is mainly caused by the normal force. The displacement in the axial direction (x direction) reaches 10^{-5} m, which is mainly caused by the axial force. The displacement in the y direction is 10^{-7} m, which is caused by the axial force and normal force.

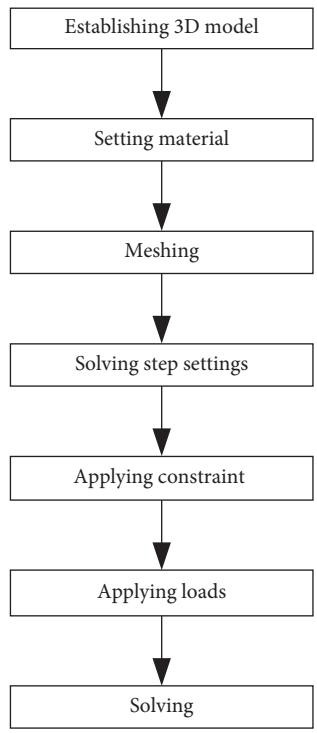

Figure 10: Simulation steps.

The total displacement is expressed as

$$d=\sqrt{d_x^2+w^2+u^2}. \tag{12}$$

The order of the displacement magnitude in the normal direction (z direction) is 10^{-4} m, and the order of the displacement magnitude in the axial direction (x direction) is 10^{-5} m. The order of the displacement magnitude in the y direction is 10^{-7} m. So, the total amplitude is simplified as

$$d\approx w. \tag{13}$$

So, the total displacement is approximately equal to the displacement in the z direction.

6. Frequency-Domain Analysis

According to equations (6) and (7), the component frequencies of axial and normal force expression can be obtained, which are listed in Table 2.

The frequency-domain distributions of the axial force and normal force can be obtained by Fourier transform of equations (6) and (7), as shown in Figure 17.

It is shown in Figure 17 that pulse values of power spectral density occur when frequencies are equal to component frequencies of axial force and normal force. The frequency-domain characteristics of axial force and normal force are similar, which means both of them have pulse values at the same frequency value.

The frequency-domain solution at the midpoint on BC as in Figure 1 can be obtained by Fourier transform of the

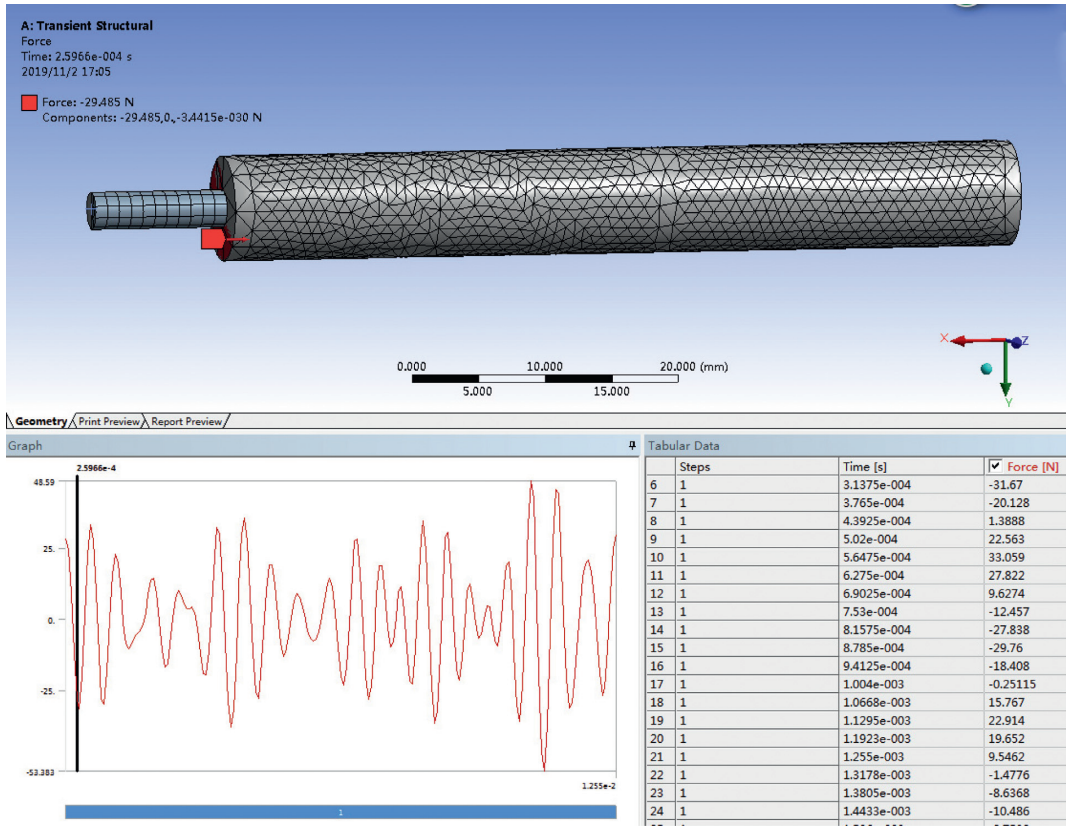

Figure 11: Imposing axial force F_a.

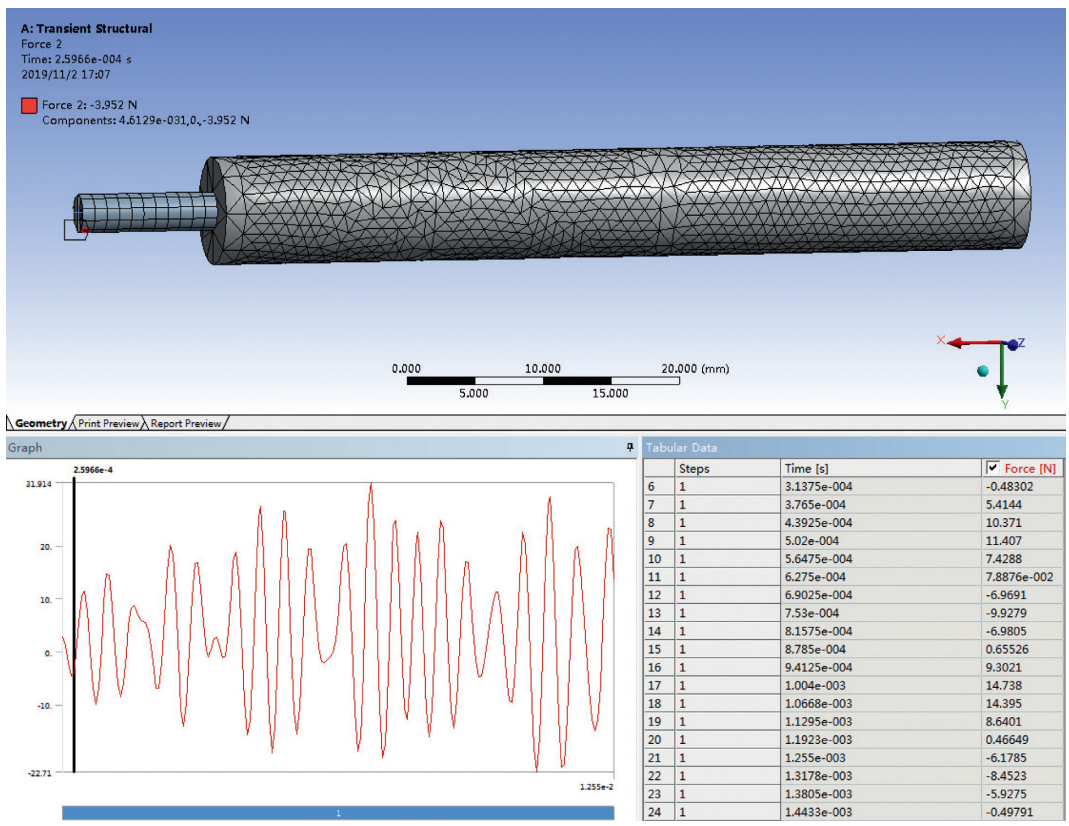

Figure 12: Imposing normal force F_n.

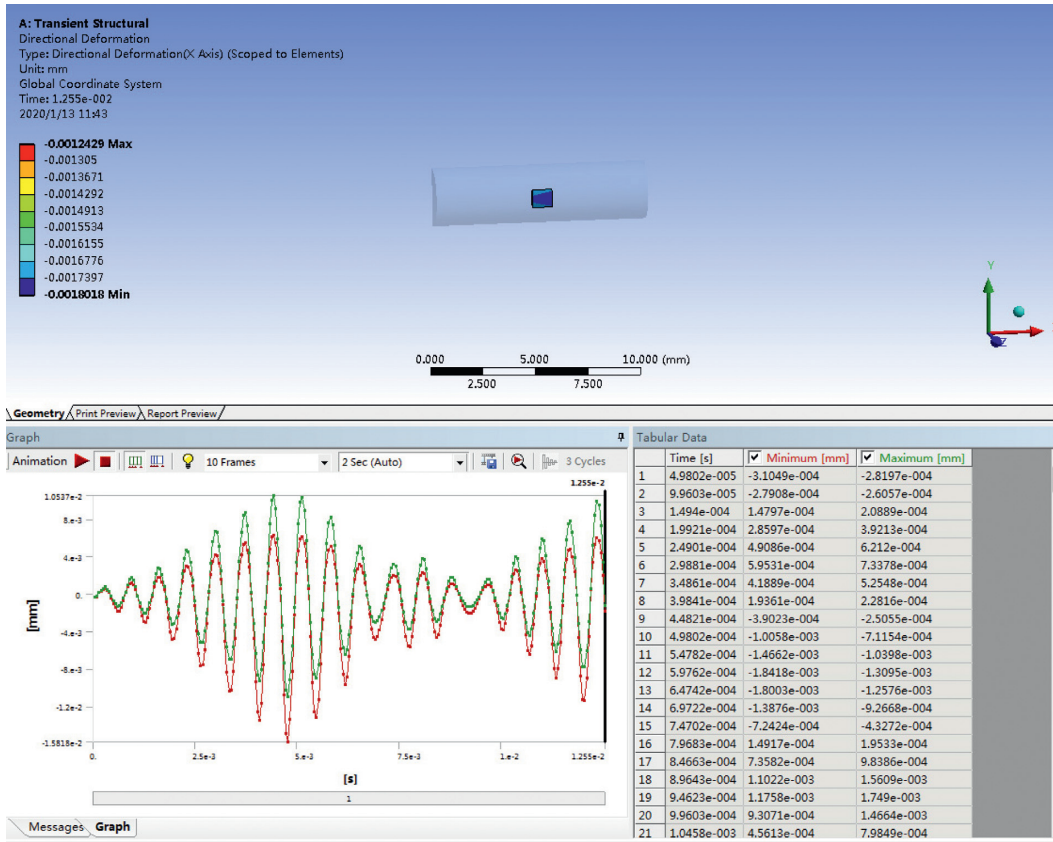

Figure 13: The solution in the x direction at the midpoint on BC.

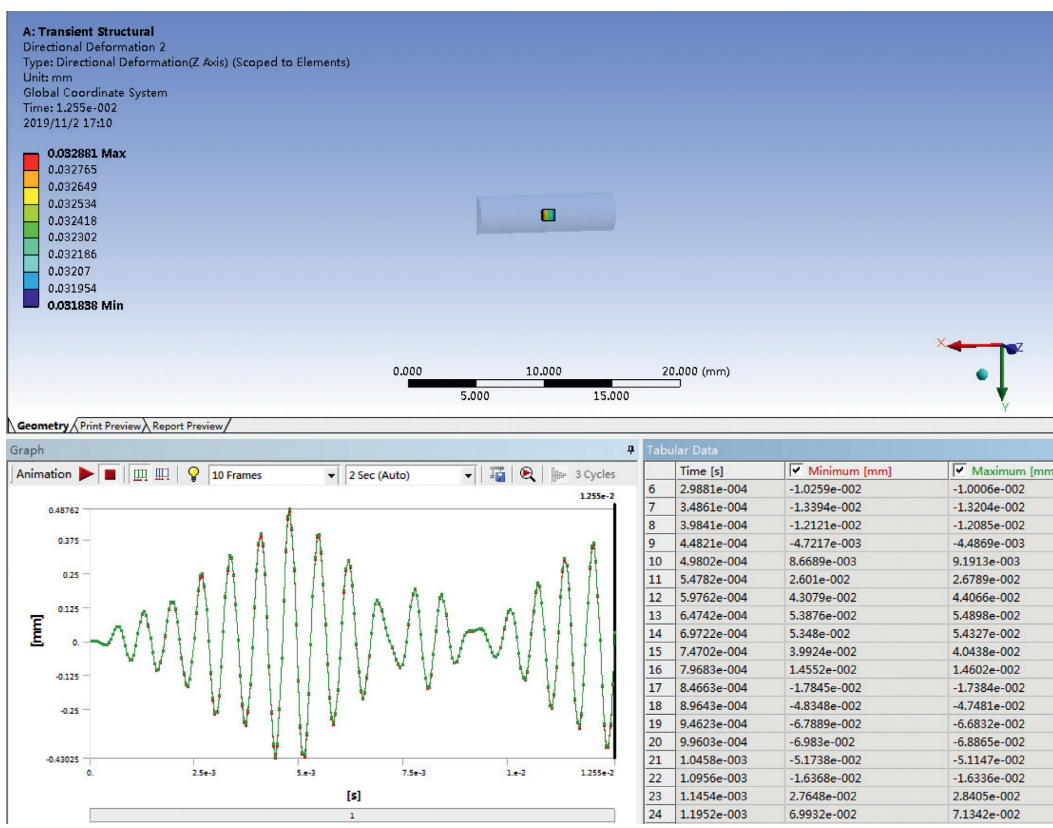

Figure 14: The solution in the z direction at the midpoint on BC.

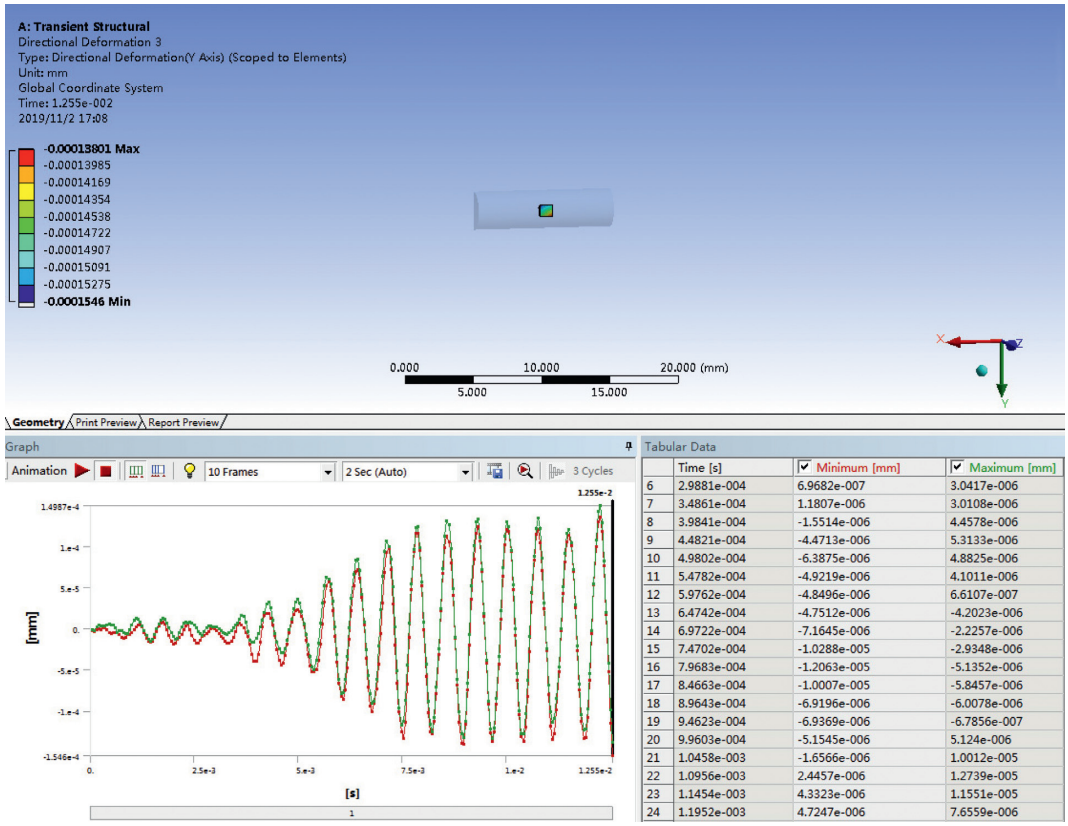

	Time [s]	Minimum [mm]	Maximum [mm]
6	2.9881e-004	6.9682e-007	3.0417e-006
7	3.4861e-004	1.1807e-006	3.0108e-006
8	3.9841e-004	-1.5514e-006	4.4578e-006
9	4.4821e-004	-4.4713e-006	5.3133e-006
10	4.9802e-004	-6.3875e-006	4.8825e-006
11	5.4782e-004	-4.9219e-006	4.1011e-006
12	5.9762e-004	-4.8496e-006	6.6107e-007
13	6.4742e-004	-4.7512e-006	-4.2023e-006
14	6.9722e-004	-7.1645e-006	-2.2257e-006
15	7.4702e-004	-1.0288e-005	-2.9348e-006
16	7.9683e-004	-1.2063e-005	-5.1352e-006
17	8.4663e-004	-1.0007e-005	-5.8457e-006
18	8.9643e-004	-6.9196e-006	-6.0078e-006
19	9.4623e-004	-6.9369e-006	-6.7856e-007
20	9.9603e-004	-5.1545e-006	5.124e-006
21	1.0458e-003	-1.6566e-006	1.0012e-005
22	1.0956e-003	2.4457e-006	1.2739e-005
23	1.1454e-003	4.3323e-006	1.1551e-005
24	1.1952e-003	4.7247e-006	7.6559e-006

Figure 15: The solution in the y direction at the midpoint on BC.

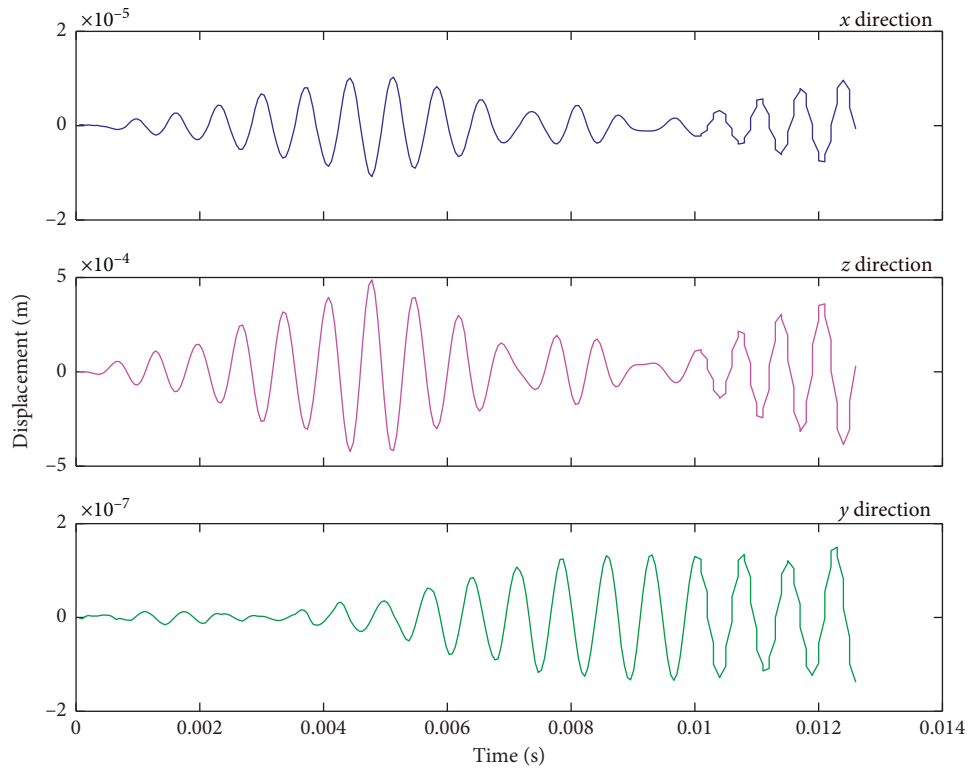

Figure 16: Time-domain solution at the midpoint on BC by simulation.

Table 2: Component frequencies of polishing force (Hz).

Component frequencies of F_a	Component frequencies of F_n
1510.7	1986.3
2002.2	33.7
1672.7	1658.4
1610.6	1609.1
1279.9	1505.8
2078.6	1871.7
1916.2	1766.6
1435.3	1279.6

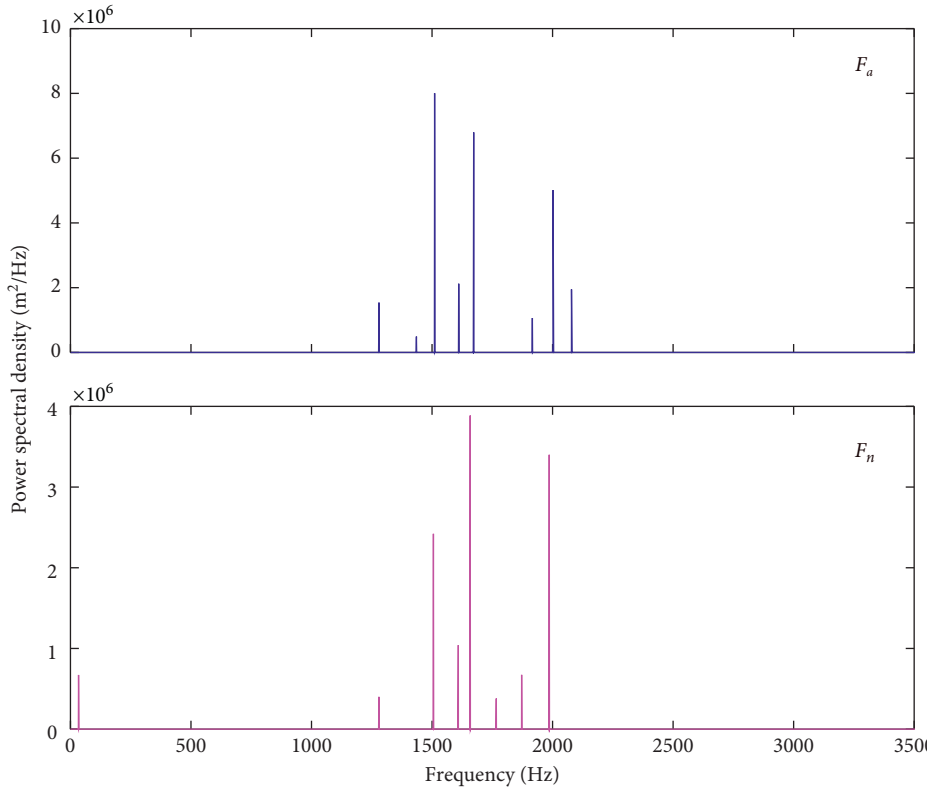

Figure 17: Frequency-domain distributions of the axial force and the normal force.

signal as shown in Figure 16. The results are shown in Figure 18.

The frequencies of the inflection point as in Figure 18 are component frequencies of rod vibration. They are listed in Table 3.

The frequency-domain characteristics of vibration in x, y, and z direction are similar, which means they occur with a peak value at the same frequency value. According to Tables 2 and 3, it is concluded that component frequencies of axial force and normal force are inconsistent with component frequencies of rod displacement vibration, which means the vibration is not stable.

By the aid of the ANSYS Workbench, modal frequencies can be obtained as shown in Table 4.

The number of abrasive belt blades of the wheel selected in this experiment is 25. In the polishing process, whenever the abrasive belt blade contacts the blade once, the polishing force signal will have a peak. So, the theoretical frequency of the force signal should be as follows:

$$f_z = \frac{n}{60} \times 25. \tag{14}$$

Figures 6 and 7 show the polishing force signals under certain process parameters, whose spindle speed is 4000 r/min and its frequency is 1666.67 Hz according to equation (14). Due to various errors, the frequency of the force signal is not 1666.67 Hz, but the force signal is the sum of sine components and the frequencies of all sine components are close to 1666.67 Hz.

When the frequency of the driving force is close to the modal frequency of the object, it is easy to produce resonance. In order to avoid resonance, the absolute value of the

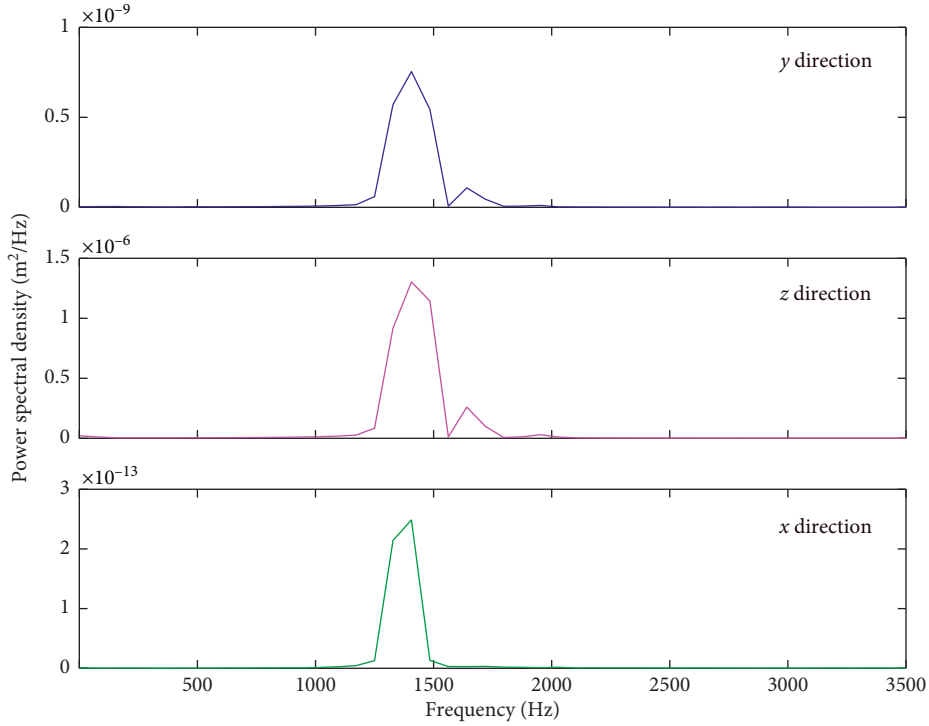

Figure 18: Frequency-domain solution at the midpoint on BC by simulation.

Table 3: Component frequencies of rod vibration (Hz).

Component frequencies of vibration in x direction	Component frequencies of vibration in y direction	Component frequencies of vibration in z direction
1250	1250	1250
1328	1328	1328
1406	1406	1406
1484	1484	1484
1641	1641	
1719	1719	

Table 4: Modal frequencies in all directions (Hz).

Mode	x direction	z direction	xy direction	yz direction	Arbitrary direction
1	21353	11215	1478.2	11214	1411
2	66468	35066	8863.7	11214	1411.1
3	112560	59901	17584	12269	8530.7
4	135650	74115	19116	35055	8533.4
5	163370	90534	25805	35056	12269
6	163370	116020	42388	37124	16933

difference between the frequency of the force and the modal frequency of the object must be greater than a certain value, which can be expressed as

$$|f_d - f_m| > f_c. \tag{15}$$

As mentioned above, when the spindle speed is 4000 r/min, the theoretical frequency of the polishing force is 1666.67 Hz, while the actual component frequencies of the polishing force are approximately 1280 Hz–2000 Hz, and the absolute value of the difference between the theoretical frequency and the actual frequencies is approximately 400 Hz. So, $f_c = 400$ Hz. It is shown that the minimum values in the low-order modal frequencies are 1411 Hz, 1411.1 Hz, and 1478.2 Hz in Table 4. In order to avoid resonance, the frequencies of polishing force f_d should conform to the inequality (15). If $f_c = 400$ Hz, the frequencies range of polishing force can be obtained as $f_d > 1878.2$ Hz or $f_d < 1011$ Hz. According to equation (14), the spindle speed range corresponding to the frequency range of polishing force is $n < 2426.4$ r/min or $n > 4507.68$ r/min. In the actual polishing process, in order to improve the polishing efficiency, the spindle speed should not be too low, so the spindle speed should be greater than 4507.68 r/min.

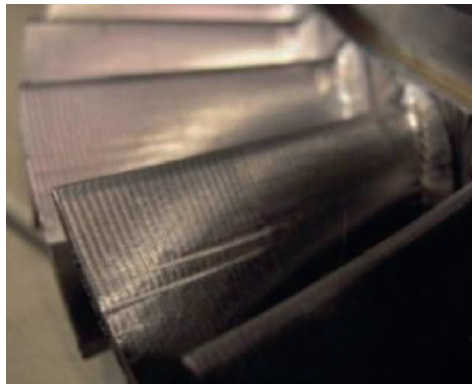

Figure 19: Blade before polishing.

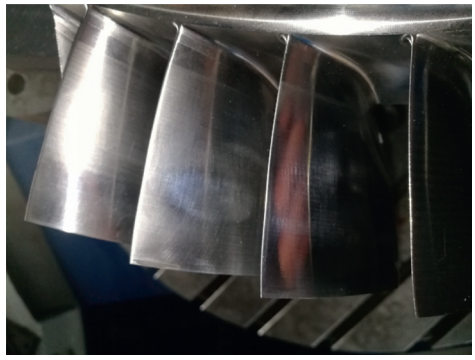

Figure 20: Blade after polishing.

Table 5: Process parameters in verification experiment.

n	a_p	v_w	P
8000	0.6	100	600

Figure 19 shows the blade after milling with a ball end milling cutter, and Figure 20 shows the blade after polishing with the process parameters in the verification experiment shown in Table 5.

7. Conclusions

It is of great significance to study polishing vibration for improving polishing process, shortening processing time, ensuring safe operation of equipment, and reducing noise pollution. In this paper, it is found that polishing vibration is not stable in the process of polishing the aeroengine blade with the abrasive cloth wheel. Therefore, it is very important to study the polishing vibration characteristics. The vibration of the polishing rod is obtained by simulation. To start with, polishing force was measured by dynamometer and it is found that polishing forces in the time domain can be expressed as the sum of sine components accurately, as equations (4) and (5). Next, time-domain and frequency-domain vibration solutions of position at which the abrasive cloth wheel is installed under the coupling of axial force and normal force are obtained by the ANSYS Workbench. The solutions show that component frequencies of polishing force are inconsistent with component frequencies of rod displacement vibration, which means the vibration is not stable. Finally, the range of spindle speed to avoid resonance in polishing process is obtained.

Nomenclature

n: Spindle speed, r/min
a_p: Compression depth, mm
v_w: Feed speed, mm/min
P: Size of the abrasive cloth wheel, #
F_X: X direction force as shown in Figure 5, N
F_Y: Y direction force as shown in Figure 5, N
F_Z: Z direction force as shown in Figure 5, N
F_n: Normal polishing force as shown in Figure 5, N
F_t: Tangential polishing force as shown in Figure 5, N
F_a: Axial polishing force as shown in Figure 5, N
t: Time, s
ρ: Density of the polishing rod, kg/m^3
$A(x)$: Cross-section area of the polished rod, m^2
$I(x)$: Inertia moment of the polishing rod to the x-axis in Figure 9, m^4
E: Elasticity modulus, Pa
u: Axial vibration displacement, m
w: Normal vibration displacement, m
d: Total vibration displacement, m
d_x: The vibration displacement in the x direction, m
f_z: Theoretical frequency of polishing force, Hz
f_d: Actual frequency of polishing force, Hz
f_m: Modal frequency of the object, Hz
f_c: Certain frequency value, Hz.

Data Availability

The data used to support the findings of this study are available from the corresponding author upon request.

Conflicts of Interest

The authors declare that they have no conflicts of interest.

Acknowledgments

This work was jointly supported by the National Natural Science Foundation, China (no. 51675439) and the National Science and Technology Major Project, China (no. 2015ZX04001003).

References

[1] R. N. Arnold, "Cutting tools research: report of subcommittee on carbide tools: the mechanism of tool vibration in the cutting of steel," *Proceedings of the Institution of Mechanical Engineers*, vol. 154, no. 1, pp. 261–284, 1946.

[2] T. Inoue and K. Hirohito, "Reasons for the return spindle," *Proceedings of the Japan Institute of Machinery*, vol. 20, no. 90, pp. 61–65, 1954.

[3] J. Tlusty and F. Ismail, "Basic non-linearity in machining chatter," *CIRP Annals-Manufacturing Technology*, vol. 30, no. 1, pp. 299–304, 1981.

[4] R. S. Hahn, "On the theory of regenerative chatter in precision grinding operations," *Transactions of ASME*, vol. 76, no. 4, pp. 593–597, 1954.

[5] F. Hashimoto, J. Yoshioka, M. Miyashita, and H. Sato, "Sequential estimation of growth rate of chatter vibration in grinding processes," *CIRP Annals*, vol. 34, no. 1, pp. 271–275, 1985.

[6] R. A. Thompson, "The character of regenerative chatter in cylindrical grinding," *Journal of Engineering for Industry*, vol. 95, no. 3, pp. 858–864, 1973.

[7] R. A. Thompson, "On the doubly regenerative stability of a grinder: the combined effect of wheel and workpiece speed," *Journal of Engineering for Industry*, vol. 99, no. 1, pp. 237–241, 1977.

[8] I. Inasaki, K. Tonou, and S. Yonetsu, "Regenerative chatter in cylindrical plunge grinding," *Bulletin of JSME*, vol. 20, no. 150, pp. 1648–1654, 1977.

[9] T. El-Wardani, M. M. Sadek, and M. A. Younis, "Theoretical analysis of grinding chatter," *Journal of Engineering for Industry*, vol. 109, no. 4, pp. 314–320, 1987.

[10] J. Biera, J. Viñolas, and F. J. Nieto, "Time-domain dynamic modelling of the external plunge grinding process," *International Journal of Machine Tools and Manufacture*, vol. 37, no. 11, pp. 1555–1572, 1997.

[11] M. Weck, N. Hennes, and A. Schulz, "Dynamic behaviour of cylindrical traverse grinding processes," *CIRP Annals*, vol. 50, no. 1, pp. 213–216, 2001.

[12] I. Inasaki, B. Karpuschewski, and H.-S. Lee, "Grinding chatter-origin and suppression," *CIRP Annals*, vol. 50, no. 2, pp. 515–534, 2001.

[13] Y. Altintas and M. Weck, "Chatter stability of metal cutting and grinding," *CIRP Annals*, vol. 53, no. 2, pp. 619–642, 2004.

[14] Z. Y. Weng, W. D. Xie, B. Lu, Y. W. Ye, H. Yao, and X. S. He, "Grinding chatter and ground surface waviness in surface grinding process," *Key Engineering Materials*, vol. 259-260, no. 3, pp. 352–356, 2004.

[15] N. Zhang, I. Kirpitchenko, and D. K. Liu, "Dynamic model of the grinding process," *Journal of Sound and Vibration*, vol. 280, no. 1-2, pp. 425–432, 2005.

[16] H. Li and Y. C. Shin, "Wheel regenerative chatter of surface grinding," *Journal of Manufacturing Science and Engineering*, vol. 128, no. 2, pp. 393–403, 2006.

[17] H. Li and Y. C. Shin, "A time-domain dynamic model for chatter prediction of cylindrical plunge grinding processes," *Journal of Manufacturing Science and Engineering*, vol. 128, no. 2, pp. 404–415, 2006.

[18] H. Li and Y. C. Shin, "A study on chatter boundaries of cylindrical plunge grinding with process condition-dependent dynamics," *International Journal of Machine Tools and Manufacture*, vol. 47, no. 10, pp. 1563–1572, 2007.

[19] Y. Yan, J. Xu, and M. Wiercigroch, "Chatter in a transverse grinding process," *Journal of Sound and Vibration*, vol. 333, no. 3, pp. 937–953, 2014.

[20] Y. Yan, J. Xu, and M. Wiercigroch, "Non-linear analysis and quench control of chatter in plunge grinding," *International Journal of Non-Linear Mechanics*, vol. 70, pp. 134–144, 2015.

[21] Y. Yan, J. Xu, and W. Wang, "Nonlinear chatter with large amplitude in a cylindrical plunge grinding process," *Nonlinear Dynamics*, vol. 69, no. 4, pp. 1781–1793, 2012.

[22] Y. Yan, J. Xu, and M. Wiercigroch, "Influence of workpiece imbalance on regenerative and frictional grinding chatters," *Procedia IUTAM*, vol. 22, pp. 146–153, 2017.

[23] Y. Yan, J. Xu, and M. Wiercigroch, "Regenerative and frictional chatter in plunge grinding," *Nonlinear Dynamics*, vol. 86, no. 1, pp. 283–307, 2016.

[24] Y. Yan, J. Xu, and M. Wiercigroch, "Regenerative chatter in a plunge grinding process with workpiece imbalance," *International Journal of Advanced Manufacturing Technology*, vol. 89, no. 9–12, pp. 2845–2862, 2017.

[25] Y. Yan, J. Xu, and M. Wiercigroch, "Regenerative chatter in self-interrupted plunge grinding," *Meccanica*, vol. 51, no. 12, pp. 3185–3202, 2016.

[26] Y. Li, S. M. Gracewski, P. D. Funkenbusch, and J. Ruckman, "Analysis of chatter in contour grinding of optical materials," *International Journal of Machine Tools and Manufacture*, vol. 42, no. 10, pp. 1095–1103, 2002.

[27] S. K. Kabini, B. W. Ikua, and G. N. Nyakoe, "Dynamic modeling of chatter vibration in cylindrical plunge grinding process," *Innovative Systems Design and Engineering*, vol. 2, no. 4, pp. 58–70, 2011.

[28] R. Entwistle and B. Stone, "Fundamental issues in self-excited chatter in grinding," *Journal of Machine Engineering*, vol. 13, no. 3, pp. 26–50, 2013.

[29] D. Hesterman and B. Stone, "Improved model of chatter in grinding, including torsional effects," *Proceedings of the Institution of Mechanical Engineers, Part K: Journal of Multi-Body Dynamics*, vol. 216, no. 2, pp. 169–180, 2002.

[30] T. Yu, Z. W. Zhang, and B. C. Wen, "Nonlinear stability and bifurcation of multi-D.O.F. Chatter system in grinding process," in *Advances in Grinding and Abrasive Technology XIII*, vol. 92, pp. 141–145, Trans Tech Publications, Stafa-Zurich, Switzerland, 2006.

[31] S. Cong, Y. J. Niu, Z. X. Liu, Y. S. Wang, and S. C. Xiu, "Study on the surface topography considering grinding chatter based on dynamics and reliability," *International Journal of Advanced Manufacturing Technology*, vol. 92, no. 9–12, pp. 3273–3286, 2017.

[32] S. J. Drew, M. A. Mannan, K. L. Ong, and B. J. Stone, "The measurement of forces in grinding in the presence of vibration," *International Journal of Machine Tools and Manufacture*, vol. 41, no. 4, pp. 509–520, 2001.

[33] N. Wang, C. Liu, D. Jiang, and K. Behdinan, "Casing vibration response prediction of dual-rotor-blade-casing system with blade-casing rubbing," *Mechanical Systems and Signal Processing*, vol. 118, pp. 61–77, 2019.

[34] N. Wang, D. Jiang, and K. Behdinan, "Vibration response analysis of rubbing faults on a dual-rotor bearing system," *Archive of Applied Mechanics*, vol. 87, no. 11, pp. 1891–1907, 2017.

[35] N. F. Wang, D. X. Jiang, and T. Han, "Dynamic characteristics of rotor system and rub-impact fault feature research based on casing acceleration," *Journal of Vibroengineering*, vol. 18, no. 3, pp. 1525–1539, 2016.

[36] H. Z. Xu, N. F. Wang, D. X. Jiang, T. Han, and D. W. Li, "Dynamic characteristics and experimental research of dual-rotor system with rub-impact fault," *Shock and Vibration*, vol. 2016, Article ID 6239281, 11 pages, 2016.

[37] E. Govekac, A. Baud, J. GradiSek, F. KlockeA, and I. Grabec, "A new method for chatter detection in grinding," *CIRP Annals-Manufacturing Technology*, vol. 51, no. 1, pp. 267–270, 2002.

[38] J. Gradisek, A. Baus, E. Govekar, F. Klocke, and I. Grabec, "Automatic chatter detection in grinding," *International Journal of Machine Tools and Manufacture*, vol. 43, no. 14, pp. 1397–1403, 2003.

[39] J. C. Fu, C. A. Troy, and K. Mori, "Chatter classification by entropy functions and morphological processing in cylindrical traverse grinding," *Precision Engineering*, vol. 18, no. 2-3, pp. 110–117, 1996.

[40] T. Zhao, Y. Y. Shi, X. J. Lin, J. H. Duan, P. C. Sun, and J. Zhang, "Surface roughness prediction and parameters optimization in grinding and polishing process for IBR of aero-engine," *International Journal of Advanced Manufacturing Technology*, vol. 74, no. 5–8, pp. 653–663, 2014.

[41] W. B. Huai, Y. Y. Shi, H. Tang, and X. J. Lin, "Prediction of surface roughness ratio of polishing blade of abrasive cloth wheel and optimization of processing parameters," *International Journal of Advanced Manufacturing Technology*, vol. 90, no. 1–4, pp. 1–10, 2016.

[42] W. Huai, Y. Shi, H. Tang, and X. Lin, "An adaptive flexible polishing path programming method of the blisk blade using elastic grinding tools," *Journal of Mechanical Science and Technology*, vol. 33, no. 7, pp. 3487–3495, 2019.

[43] C. Xian, Y. Y. Shi, X. J. Lin, and D. Liu, "Experimental study on energy partition of polishing aero-engine blades with abrasive cloth wheel," *International Journal of Advanced Manufacturing Technology*, vol. 106, no. 5-6, pp. 1839–1853, 2020.

[44] C. Xian, Y. Y. Shi, X. J. Lin, and D. Liu, "Force modeling for polishing aero-engine blades with abrasive cloth wheels," *International Journal of Advanced Manufacturing Technology*, vol. 106, no. 11-12, pp. 5255–5267, 2020.

[45] G. J. Xiao, Y. He, Y. Huang, and Q. Li, "Shark-skin-inspired micro-riblets forming mechanism of TC17 titanium alloy with belt grinding," *IEEE Access*, vol. 35, no. 1, pp. 107636–107648, 2019.